Statistically linearized optimal control of an electromagnetic vibratory energy harvester

Statistically linearized optimal control of an electromagnetic vibratory energy harvester

Ian L Cassidy[1] and Jeffrey T Scruggs[2]

[1] Department of Civil and Environmental Engineering, Duke University, Durham, NC 27708, USA
[2] Department of Civil and Environmental Engineering, University of Michigan, Ann Arbor, MI 41209, USA

E-mail: ian.cassidy@duke.edu and jscruggs@umich.edu

Abstract
In this paper, an extension of linear-quadratic-Gaussian (LQG) control theory is used to
determine the optimal state feedback controller for a vibratory energy harvesting system with
Coulomb friction. Specifically, the energy harvester is a base-excited
single-degree-of-freedom (SDOF) resonant oscillator with an electromagnetic transducer
attached between the base and the moving mass. The development of the optimal controller
for this system is based on statistical linearization, whereby the Coulomb friction force is
replaced by an equivalent linear viscous damping term, which is calculated from the stationary
covariance of the closed-loop system. It is shown that the covariance matrix and optimal
feedback gain matrix can be computed by implementing an iterative algorithm involving linear
matrix inequalities (LMIs). Furthermore, this theory is augmented to account for a
non-quadratic dissipation in the electronics used to control the energy conversion. Simulation
results are presented for the SDOF energy harvester in which the performance of the optimal
state feedback control law is compared to the performance of the optimal static admittance
over a range of disturbance bandwidths.

1. Introduction

Electromechanical systems to harvest energy from ambient mechanical vibrations have become the subject of considerable engineering research. For applications in which the power requirements are on the order of μW–mW, the dominant technology has been comprised of piezoelectric transducers embedded within flexible cantilever beams. For example, it has been shown in several studies that such piezoelectric transducers can be used to power wireless sensing and embedded computing systems [1–3]. However, large-scale energy harvesting from vibrating structures (i.e., vehicles, multi-story buildings, and bridges) has recently also been shown to be a viable source of renewable energy. Electromagnetic transducers have been developed to extract power from vibrations in automotive suspensions [4], railway systems [5], wave excitations on offshore structures [6], and

wind excitations on buildings [7]. The available power from such applications has been estimated to be at the W–kW scale.

Regardless of the scale or the hardware that is being used to harvest energy, nonlinearities often exist in the vibrating structure and transducer. In a recent study by Stanton *et al* [8], a nonlinear model for a piezoelectric energy harvester is derived from first principles and is compared to an experimental system. It is shown that nonlinear damping in the cantilever beam as well as nonlinear electromechanical coupling in the piezoelectric patch must be accounted for in the model in order to accurately predict the response of the beam. In addition, Cassidy *et al* [9] developed a predictive model to account for the nonlinearities present in an electromagnetic transducer consisting of a ballscrew actuator coupled to a permanent-magnetic synchronous machine. The nonlinearities in that device are caused by the sliding friction interaction between the ballscrew and ball bearings as well as

the elasticity of the belt that connects the ballscrew to the shaft of the motor.

Nonlinearities also occur in the electronics that interface the transducer with energy storage. For the simplest passive energy harvesting circuit, which consists of a standard diode bridge, a small amount of parasitic power is dissipated in a nonlinear manner as a result of the voltage threshold that is required for the diodes to conduct. More elaborate active energy harvesting circuits, such as buck–boost converters [10] or H-bridges [11, 12], are operated via high-frequency pulsewidth modulated (PWM) switching control of MOSFETs. The parasitic power losses associated with these switching converters are highly nonlinear and are a result of the way in which the transducer current is controlled to track a desired current. As such, the study by Scruggs *et al* [13] derived an approximate loss model for the behavior of an H-bridge operated in discontinuous conduction for a piezoelectric energy harvester excited by a broadband disturbance. The nonlinearities in the model derived in that paper can be attributed to the conduction losses in the MOSFETs and diodes as well as gating and transition losses.

Despite the challenges associated with modeling nonlinear power losses in switching converters, it has been demonstrated that these circuits have many advantages over the standard passive diode bridge. The main advantage of switching converters is that they can impose desired static or dynamic relationships between the voltage and current of the transducer. As such, the input admittance of the circuit can be freely chosen to optimize the rate of power flow from the transducer to storage. Several studies [14, 15] have shown that for sinusoidal disturbances, power generation is optimized by matching the input admittance of the harvesting circuit to the complex conjugate transpose of the driving point admittance of the harvester. For the case in which the energy harvester is excited by a stochastic disturbance, Scruggs showed in [15] that the optimal causal control of the transducer current (as derived by LQG control theory) is such that the input admittance of the optimal harvesting circuit cannot be made equivalent to any passive network. This is because in such circumstances, there are frequency bands in which the average power for the optimized system flows from storage back into the harvester. That study advocates for the realization of a synthetic dynamic admittance using an actively controlled H-bridge.

The main objective of this paper is to develop a way to account for dynamic nonlinearities in the harvester, while optimizing the controller for maximum power generation. Toward this end we use statistical linearization to account for the influence of the nonlinearities on the stochastic response. This concept has been applied in piezoelectric energy harvesting applications by Ali *et al* [16], but not in the context of optimal control. However, problems involving simultaneous statistical linearization and optimal control have been investigated in other applications. These techniques were first developed to account for saturation constraints on control inputs in stochastic systems [17]. In another study by Gökçek *et al* [18], saturating linear-quadratic-regulator (SLQR) and

saturating linear-quadratic-Gaussian (SLQG) feedback gains were developed for linear systems with saturating actuators. Several additional studies [19–21] have developed sub-optimal control designs to account for nonlinear systems that are subjected to stochastic disturbances. In [19], an iterative algorithm was proposed in which the optimal controller for the statistically linearized system is updated until specified response statistics converge. However, a standard Riccati equation is solved for the statistically linearized system at each iteration, which results in the performance being sub-optimal. Controllers developed for the systems studied in [20, 21] were computed by first statistically linearizing the nonlinear system, and then solving a standard Riccati equation as if the linearized coefficients were independent of the feedback law. This also leads to a sub-optimal solution.

In this paper, the control objective is different from the ones presented in [17–21]. The performance objective in those studies minimizes the variance of the system's output, while the performance objective in the present study maximizes the average power generated by the transducer. Furthermore, the nonlinearity in the energy harvesting system in this study is a result of Coulomb friction present in the electromagnetic transducer, which was experimentally identified in [9]. We show that the optimal feedback gains for the nonlinear system can be computed by solving two nonlinear, coupled algebraic equations. The first equation is similar to the standard Lyapunov equation, which is used to solve for the stationary covariance matrix, while the second equation is similar to the standard Riccati equation, which is used to solve for the optimal feedback gains. Solving these two equations can be accomplished through an iterative algorithm, which solves the Riccati equation using standard linear matrix inequality (LMI) [22] techniques. In addition to the nonlinearities in the transducer, we develop a non-quadratic loss model for the H-bridge operating in continuous conduction mode (CCM). The final section of this paper augments the iterative algorithm to account for this non-quadratic loss model in the optimization of the controller.

2. Energy harvester model

An illustration of the electromagnetic transducer that is considered in this study is shown in figure 1(a). Linear-to-rotational conversion is accomplished via a precision ballscrew. Such devices constitute one of the most efficient methods of linear-to-rotational conversion when power flow is in the direction from linear-to-rotational motion and when high mechanical advantage is important. The ballscrew is interfaced with the shaft of a permanent magnet synchronous machine via a timing belt with a 1:1 ratio. Typically, these types of transducers are used for positioning in the manufacturing industry and are commercially available, for example, from Kollmorgen [23, 24].

The linear velocity $\dot{r}(t)$ of the device is related to the angular velocity of the motor $\dot{\theta}(t)$ via the lead conversion l; i.e., $\dot{r}(t) = l\dot{\theta}(t)$. The linear-to-rotational conversion of the ballscrew can be modeled as relating the linear force $f(t)$ of

(a)

(b)
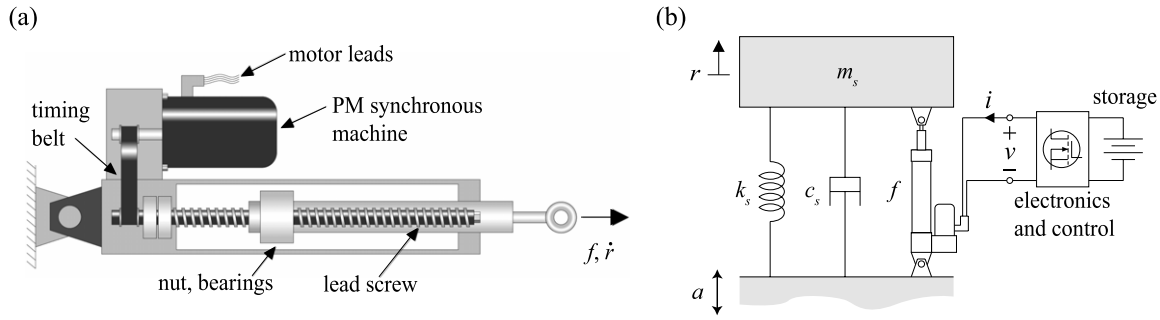
Figure 1. (a) Illustration of the electromagnetic transducer, consisting of a back-driven ballscrew and a permanent magnet synchronous machine; (b) SDOF oscillator and coupled electromagnetic transducer, which is connected to electronics and energy storage.

the device to the electromechanical force $f_e(t)$ of the motor, via the equation

$$f(t) = f_e(t) - F_c \text{sgn}(\dot{r}(t)) - m_d \ddot{r}(t) - c_d \dot{r}(t) - k_d r(t) \quad (1)$$

where m_d and c_d are the equivalent linear mass and viscous damping resulting from the rotational inertia and viscous damping of the ballscrew and shaft of the motor, respectively. It was experimentally determined in Cassidy *et al* [9] that Coulomb friction and stiffness forces, which are represented by F_c and k_d, are also present in the device. In addition, it is shown in [9] that the electromechanical force for the transducer considered in this study is proportional to current via the relationship

$$f_e(t) = \frac{3K_e}{2l} i(t) = c_e i(t) \quad (2)$$

where K_e is the magnitude of the back-emf of the motor and c_e is the electromechanical coupling coefficient. From the relationship in equation (2), the voltage generated by the transducer is proportional to linear velocity; i.e., $v(t) = c_e \dot{r}(t)$.

Next, we consider an energy harvesting system consisting of the electromagnetic transducer embedded within a single-degree-of-freedom (SDOF) resonant oscillator as shown in figure 1(b). The SDOF oscillator is characterized by a mass m_s, a damping c_s, and a stiffness k_s, and is excited at its base by the stochastic disturbance acceleration $a(t)$. Thus, the coupled dynamics of the SDOF oscillator and electromagnetic transducer can be expressed by the nonlinear differential equation

$$m\ddot{r}(t) + c\dot{r}(t) + kr(t) + F_c \text{sgn}(\dot{r}(t)) = m_s a(t) + f_e(t) \quad (3)$$

where $r(t)$ is the relative displacement of the mass of the structure, $m = m_d + m_s$, $c = c_d + c_s$, and $k = k_d + k_s$. If we define the harvester state vector as $\mathbf{x}_h(t) = [\sqrt{k}r(t) \ \sqrt{m}\dot{r}(t)]^T$, then the harvester dynamics can be expressed by the self-dual state space

$$\dot{\mathbf{x}}_h(t) = \mathbf{A}_h \mathbf{x}_h(t) + \mathbf{F}_h \text{sgn}(\dot{r}(t)) + \mathbf{B}_h i(t) + \mathbf{G}_h a(t) \quad (4a)$$

$$v(t) = \mathbf{B}_h^T \mathbf{x}_h(t) \quad (4b)$$

$$\dot{r}(t) = \mathbf{C}_h \mathbf{x}_h(t) \quad (4c)$$

where

$$\mathbf{A}_h = \begin{bmatrix} 0 & \sqrt{k/m} \\ -\sqrt{k/m} & -c/m \end{bmatrix}, \qquad \mathbf{B}_h = \begin{bmatrix} 0 \\ c_e/\sqrt{m} \end{bmatrix},$$
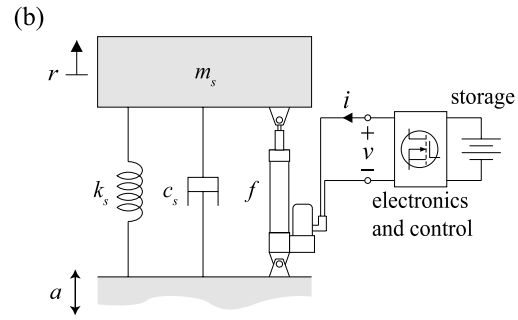
$$\mathbf{G}_h = \begin{bmatrix} 0 \\ m_s/\sqrt{m} \end{bmatrix},$$

$$\mathbf{F}_h = \begin{bmatrix} 0 \\ -F_c/\sqrt{m} \end{bmatrix}, \qquad \mathbf{C}_h = \begin{bmatrix} 0 & 1/\sqrt{m} \end{bmatrix}.$$

In many vibratory energy harvesting applications, the disturbance acceleration is most accurately modeled as a broadband stochastic process. As such, we characterize the disturbance acceleration by the second-order bandpass filter

$$\dot{\mathbf{x}}_a(t) = \mathbf{A}_a \mathbf{x}_a(t) + \mathbf{B}_a w(t) \quad (5a)$$

$$a(t) = \mathbf{C}_a \mathbf{x}_a(t) \quad (5b)$$

where

$$\mathbf{A}_a = \begin{bmatrix} 0 & 1 \\ -\omega_a^2 & -2\zeta_a\omega_a \end{bmatrix}, \qquad \mathbf{B}_a = \begin{bmatrix} 0 \\ 2\sigma_a\sqrt{\zeta_a\omega_a} \end{bmatrix},$$

$$\mathbf{C}_a = \begin{bmatrix} 0 & 1 \end{bmatrix}.$$

We assume that the input $w(t)$ is a white noise process with spectral intensity equal to unity. In addition, we have that σ_a is the standard deviation of the disturbance acceleration, $\omega_a = \sqrt{k/m}$ is the passband of disturbance filter, and ζ_a determines the quality factor of the disturbance filter. We combine the harvester states with the disturbance states such that the augmented state space $\mathbf{x}(t) = \begin{bmatrix} \mathbf{x}_h^T(t) & \mathbf{x}_a^T(t) \end{bmatrix}^T$ obeys

$$\dot{\mathbf{x}}(t) = \mathbf{A}\mathbf{x}(t) + \mathbf{F}\text{sgn}(\dot{r}(t)) + \mathbf{B}i(t) + \mathbf{G}w(t) \quad (6a)$$

$$v(t) = \mathbf{B}^T \mathbf{x}(t) \quad (6b)$$

$$\dot{r}(t) = \mathbf{C}\mathbf{x}(t) \quad (6c)$$

with appropriate definitions for the matrices $\{\mathbf{A}, \mathbf{B}, \mathbf{C}, \mathbf{F}, \mathbf{G}\}$ above.

Values for the various parameters considered in this study can be found in table 1. The transducer parameter values are specific to the EC3 ballscrew and AKM44E motor configuration from Kollmorgen, which were experimentally verified in Cassidy *et al* [9]. In addition, the energy harvester's mass, damping, and stiffness correspond to values for a scaled tuned mass damper within a multi-story building. The system's natural frequency is 0.5 Hz, with a damping ratio of 5%.

3
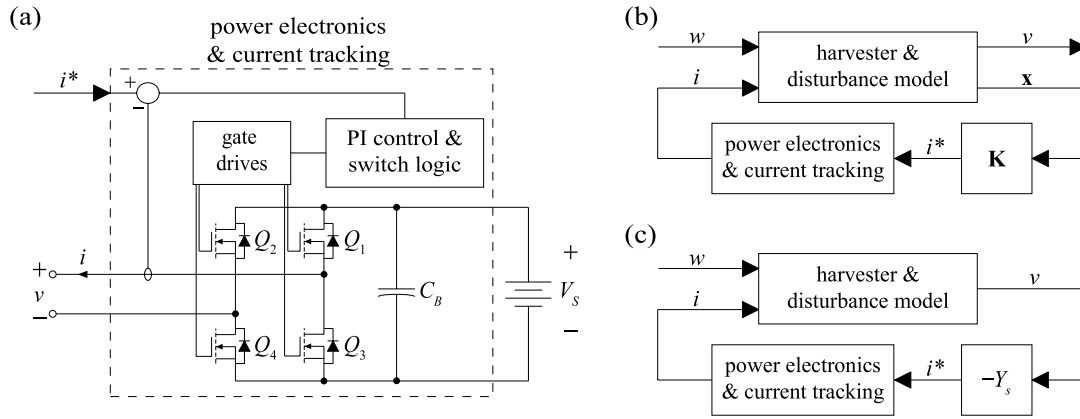
Figure 2. (a) Example power electronic circuit consisting of an H-bridge; (b) block diagram illustrating the state feedback control law; (c) block diagram illustrating the static admittance.

Table 1. Parameter values for the electromagnetic energy harvester.

Parameter	Value	Parameter	Value
K_e	0.77 N m A^{-1}	F_c	160 N
R_c	2.41 Ω	m_s	3000 kg
l	2.55×10^{-3} m rad^{-1}	c_s	395 N s m^{-1}
m_d	20 kg	k_s	3×10^4 N s^{-1}
c_d	575 N s m^{-1}	ω_a	0.5 Hz
k_d	630 N m^{-1}	σ_a	0.18 m s^{-2}

3. Optimal linear energy harvesting

In this section, we neglect the effects of the Coulomb friction force in equation (6) (i.e., we assume that $F_c = 0$). In addition, we assume that the power losses in the electronics are quadratic and purely resistive. For the linear harvester and disturbance model, it is then possible to determine the state feedback control law that maximizes the harvested power using LQG optimal control theory. Optimization of the energy harvesting cost function can be accomplished through the linear state feedback relationship $i(t) = \mathbf{K}\mathbf{x}(t)$, where the matrix $\mathbf{K}$ can be computed as explained below.

Operating the transducer such that it implements a desired control law requires power electronic circuitry to accurately track a current command signal. Because the electronics must be capable of injecting as well as extracting power, an H-bridge, which is pictured in figure 2(a), is used to track the current command signal $i^*(t)$. As shown in figure 2(a), tracking $i^*(t)$ is accomplished through high-frequency pulsewidth modulation (PWM) switching control of four MOSFETs (labeled Q_1 through Q_4). Gate drives control the MOSFETs using an error signal, which is computed by sending the difference between the desired and actual current through a proportional–integral (PI) controller. We make the assumption that the tracking dynamics of the power electronics lie outside the frequency band of the disturbance.

To determine the energy harvesting cost function, we first define the power delivered to storage as the power extracted by the transducer minus the transmission losses in

the power electronic circuitry. If we approximate these losses as resistive, with some resistance R, then the power delivered to storage is $P_S(t) = -i(t)v(t) - Ri^2(t)$. We note that the negative signs in this expression are due to the fact that the current flowing into the transducer is defined as being positive in figure 2(a). Next, we define the average power generated as the expectation of the power delivered to storage; i.e.,

$$\bar{P}_{gen} = -\mathcal{E}\left\{ \begin{bmatrix} \mathbf{x}(t) \\ i(t) \end{bmatrix}^T \begin{bmatrix} \mathbf{0} & \frac{1}{2}\mathbf{B} \\ \frac{1}{2}\mathbf{B}^T & R \end{bmatrix} \begin{bmatrix} \mathbf{x}(t) \\ i(t) \end{bmatrix} \right\}. \quad (7)$$

Maximization of equation (7) is equivalent to a LQG optimal control problem.

In order to maximize the expression in equation (7), we must determine the optimal feedback gain matrix $\mathbf{K}$. It has been shown in [15] that $\mathbf{K}$ is

$$\mathbf{K} = -\frac{1}{R}\mathbf{B}^T\left(\mathbf{P} + \frac{1}{2}\mathbf{I}\right) \quad (8)$$

where $\mathbf{P} = \mathbf{P}^T < 0$ is the unique, stabilizing solution to the nonstandard Riccati equation

$$\mathbf{A}^T\mathbf{P} + \mathbf{P}\mathbf{A} - \frac{1}{R}\left(\mathbf{P} + \frac{1}{2}\mathbf{I}\right)\mathbf{B}\mathbf{B}^T\left(\mathbf{P} + \frac{1}{2}\mathbf{I}\right) = \mathbf{0}. \quad (9)$$

Furthermore, the average power generated with the electronics implementing the optimal feedback control law is

$$\bar{P}_{gen} = -\mathbf{G}^T\mathbf{P}\mathbf{G}. \quad (10)$$

A block diagram illustrating the implementation of the optimal state feedback control law can be seen in figure 2(b). In this figure, we make the assumption that $i(t) \approx i^*(t)$. In addition, we assume that every state in the augmented harvester and disturbance model is available for feedback. However, if this is not the case, then the measured transducer voltage can be passed through a standard Luenberger observer [25], which can be used to estimate the remaining system states. It would thus be straightforward to extend the theory presented in this paper to design a dynamic controller that maps the transducer voltage into the current command signal to be tracked by the electronics.

It is also possible to operate the H-bridge such that it imposes a static admittance at the terminals of the transducer. By convention, when the electronics are implementing the static admittance the control current relationship is $i(t) = -Y_s v(t)$. A block diagram illustrating the implementation of the static admittance can be seen in figure 2(c). Again, we make the assumption that $i(t) \approx i^*(t)$. If we substitute $i(t) = -Y_s v(t)$ into equation (6), then the stationary covariance matrix $\mathbf{S} = \mathcal{E}\{\mathbf{x}\mathbf{x}^T\}$ is found by solving the Lyapunov equation

$$[\mathbf{A} - Y_s \mathbf{B}\mathbf{B}^T]\mathbf{S} + \mathbf{S}[\mathbf{A} - Y_s \mathbf{B}\mathbf{B}^T]^T + \mathbf{G}\mathbf{G}^T = \mathbf{0} \quad (11)$$

and the resultant average power generated can be computed as

$$\bar{P}_{gen} = (Y_s - Y_s^2 R)\mathbf{B}^T \mathbf{S}\mathbf{B}. \quad (12)$$

Because the system only has one design parameter (i.e., Y_s) in this case, the most straightforward way to optimize $\bar{P}_{gen}$ is via a one-dimensional line search. For example, the bisection algorithm will converge rapidly to the optimal Y_s, given $\{\mathbf{A}, \mathbf{B}, \mathbf{G}, R\}$.

4. Statistically linearized energy harvesting

In this section, we extend the theory presented in the previous section to account for the Coulomb friction force present in the electromagnetic transducer. Again we assume that the losses in the electronics are purely resistive.

4.1. Stationary covariance

The general state space model for an energy harvesting system with nonlinearities is

$$\dot{\mathbf{x}}(t) = \mathbf{A}\mathbf{x}(t) + \phi(\mathbf{x}(t), t) + \mathbf{B}i(t) + \mathbf{G}w(t) \quad (13a)$$

$$v(t) = \mathbf{B}^T \mathbf{x}(t) \quad (13b)$$

$$y(t) = \mathbf{C}\mathbf{x}(t) \quad (13c)$$

where we assume the function $\phi(\mathbf{x}(t), t)$ is nonlinear. We assume $\phi(\mathbf{0}, t) = \mathbf{0}$, and that it is anti-symmetric; i.e., $\phi(-\mathbf{x}(t), t) = -\phi(\mathbf{x}(t), t)$. In addition, we assume that $\mathbf{x}(t)$ has a probability distribution which can be approximated as Gaussian with zero mean (because $\phi(\mathbf{x}(t), t)$ is assumed to be anti-symmetric) and covariance $\mathbf{\Sigma}(t)$. The corresponding probability density function (pdf) of $\mathbf{x}(t)$ is

$$p(\mathbf{x}(t), t) = \frac{1}{\sqrt{(2\pi)^n \det \mathbf{\Sigma}(t)}} \exp\left\{-\frac{1}{2}\mathbf{x}^T(t)\mathbf{\Sigma}^{-1}(t)\mathbf{x}(t)\right\}. \quad (14)$$

If we implement any stabilizing full-state feedback control law $i(t) = \mathbf{K}\mathbf{x}(t)$, then the solution to the covariance $\mathbf{\Sigma}(t)$ can be found via statistical linearization [26]. Specifically, the dynamic evolution of $\mathbf{\Sigma}(t)$ is governed by the differential equation

$$\dot{\mathbf{\Sigma}}(t) = \mathcal{E}\{\nabla_{\mathbf{x}}^T \phi_{cl}^T(\mathbf{x}(t), t)\}^T \mathbf{\Sigma}(t)$$
$$+ \mathbf{\Sigma}(t)\mathcal{E}\{\nabla_{\mathbf{x}}^T \phi_{cl}^T(\mathbf{x}(t), t)\} + \mathbf{G}\mathbf{G}^T \quad (15)$$

where the closed-loop nonlinear function $\phi_{cl}(\mathbf{x}(t), t)$ is

$$\phi_{cl}(\mathbf{x}(t), t) = \mathbf{A}\mathbf{x}(t) + \mathbf{B}\mathbf{K}\mathbf{x}(t) + \phi(\mathbf{x}(t), t) \quad (16)$$

and where $\nabla_{\mathbf{x}}$ is the gradient operator with respect to the variable $\mathbf{x}$. The covariances, $\mathbf{S}$, in stationary response is then found by finding the equilibrium of the above, i.e., the solution to the Lyapunov-like equation

$$\mathcal{E}\{\nabla_{\mathbf{x}}^T \phi_{cl}^T(\mathbf{x})\}^T \mathbf{S} + \mathbf{S}\mathcal{E}\{\nabla_{\mathbf{x}}^T \phi_{cl}^T(\mathbf{x})\} + \mathbf{G}\mathbf{G}^T = \mathbf{0}. \quad (17)$$

For the case where the nonlinearity is Coulomb friction, we replace $\phi(\mathbf{x}(t), t)$ with $\mathbf{F}\text{sgn}\{\dot{r}(t)\}$ in equation (16) where $\dot{r}(t) = y(t)$. Taking the gradient of $\phi_{cl}(\mathbf{x}(t), t)$ with respect to $\mathbf{x}(t)$, results in

$$\nabla_{\mathbf{x}}^T \phi_{cl}^T(\mathbf{x}(t), t) = \mathbf{A}^T + \mathbf{K}^T \mathbf{B}^T + 2\mathbf{C}^T \mathbf{F}^T \delta(y(t)) \quad (18)$$

where $\delta(\cdot)$ is the Dirac delta function. Next, taking the expectation of both sides of equation (18) results in the following expression

$$\mathcal{E}\{\nabla_{\mathbf{x}}^T \phi_{cl}^T(\mathbf{x}(t), t)\} = \mathbf{A}^T + \mathbf{K}^T \mathbf{B}^T$$
$$+ 2\mathbf{C}^T \mathbf{F}^T \int_y \delta(y(t))p(y(t), t)\, dy. (19)$$

But by assumption, the pdf for $y(t)$ is a zero-mean Gaussian function, with scalar variance $\sigma_y(t) = \mathbf{C}\mathbf{\Sigma}(t)\mathbf{C}^T$; i.e.,

$$p(y(t), t) = \frac{1}{\sqrt{2\pi\sigma_y(t)}} \exp\{-y^2(t)/2\sigma_y(t)\}. \quad (20)$$

Thus, we have that equation (19) is

$$\mathcal{E}\{\nabla_{\mathbf{x}}^T \phi_{cl}^T(\mathbf{x}(t), t)\} = \mathbf{A}^T + \mathbf{K}^T \mathbf{B}^T + \mathbf{V}(t)^T \quad (21)$$

where

$$\mathbf{V}(t) = \sqrt{\frac{2}{\pi}} \frac{\mathbf{F}\mathbf{C}}{\sqrt{\mathbf{C}\mathbf{\Sigma}(t)\mathbf{C}^T}}. \quad (22)$$

Substituting equation (21) into (15) results in an equation for $\mathbf{\Sigma}(t)$ as

$$\dot{\mathbf{\Sigma}}(t) = \mathbf{A}_{cl}(t)\mathbf{\Sigma}(t) + \mathbf{\Sigma}(t)\mathbf{A}_{cl}(t)^T + \mathbf{G}\mathbf{G}^T \quad (23)$$

where $\mathbf{A}_{cl}(t) = \mathbf{A} + \mathbf{B}\mathbf{K} + \mathbf{V}(t)$. It is important to note that the matrix $\mathbf{V}(t)$ augments the dynamics matrix $\mathbf{A}$ by adding an additional term which supplements the viscous damping in the system. This additional term is the statistically equivalent linear viscous damping due to the Coulomb friction force.

The stationary covariance is then the equilibrium solution of equation (23); i.e., the solution with $\dot{\mathbf{\Sigma}}(t) = \mathbf{0}$. Although the resultant equation is reminiscent of an algebraic Lyapunov equation, it is in fact nonlinear, because $\mathbf{V}(t)$ depends on $\mathbf{\Sigma}(t)$. In general, the equilibrium solution to equation (23) can only be found iteratively.

It is also important to recognize that equilibrium solutions of equation (23) may not necessarily be stable, and mean-square stability of any equilibrium solution must be checked. From classical linear system theory, we know that if $\mathbf{A}_{cl}(t)$ were constant (i.e., if it did not depend on $\mathbf{\Sigma}(t)$)

then equation (23) would have a unique equilibrium, so long as $\mathbf{A}_{\text{cl}}(t)$ does not have any two eigenvalues that sum to zero. Asymptotic stability of this unique equilibrium (and, therefore, achievement of stationarity of the covariance $\Sigma(t)$) then follows if and only if $\mathbf{A}_{\text{cl}}(t)$ is asymptotically stable. However, because $\mathbf{A}_{\text{cl}}(t)$ varies with $\Sigma(t)$, the situation at hand is somewhat more complicated than this.

Let $\mathbf{S}$ be an equilibrium solution to equation (23), and then consider that for $\|\Sigma(t) - \mathbf{S}\|$ small, the stability of $\Sigma(t)$ can be ascertained by examining the linearized version of equation (23), with $\Sigma(t) = \mathbf{S}$ used as the linearization point. The resultant linearized covariance equation for the deviation $\Xi(t) = \Sigma(t) - \mathbf{S}$ is

$$\dot{\Xi}(t) = \mathbf{A}_{\text{cl}}\Xi(t) + \Xi(t)\mathbf{A}_{\text{cl}}^{\text{T}}$$
$$- \sqrt{\frac{1}{2\pi}} \frac{\mathbf{C}\Xi(t)\mathbf{C}^{\text{T}}}{(\mathbf{C}\mathbf{S}\mathbf{C}^{\text{T}})^{3/2}}[\mathbf{FCS} + \mathbf{SC}^{\text{T}}\mathbf{F}^{\text{T}}] \quad (24)$$

where the time-invariant closed-loop dynamics matrix is $\mathbf{A}_{\text{cl}} = \mathbf{A}_{\text{cl}}(t)|_{\Sigma(t)=\mathbf{S}}$. In order for equilibrium solution $\mathbf{S}$ to be a valid stationary solution, the above linearized differential equation must be asymptotically stable about the origin.

Note that equation (24) is not a standard Lyapunov differential equation, due to the last term on the right. Similar equations arise in the literature on stochastic systems with multiplicative noise inputs [27], where it is well known that asymptotic stability is not in general guaranteed by asymptotic stability of $\mathbf{A}_{\text{cl}}$. Even when this condition is satisfied, the last term on the right-hand side can have a destabilizing effect. For a given set of parameters $\{\mathbf{A}, \mathbf{B}, \mathbf{C}, \mathbf{F}, \mathbf{K}\}$ and a known equilibrium solution $\mathbf{S}$, stability of equation (24) can be inferred exactly by converting this equation into vectorized form, using Kronecker algebra, and then examining the asymptotic stability of associated $n^2 \times n^2$ dynamics matrix. However, here we instead introduce a simpler test that is sufficient to guarantee stationarity. Specifically it can be shown that if $\mathbf{A}_{\text{cl}}$ is asymptotically stable and if

$$\frac{(\mathbf{C}\mathbf{S}\mathbf{T}\mathbf{S}\mathbf{C}^{\text{T}})^{1/2}(\mathbf{F}^{\text{T}}\mathbf{T}\mathbf{F})^{1/2}}{(\mathbf{C}\mathbf{S}\mathbf{C}^{\text{T}})^{3/2}} < \sqrt{\frac{\pi}{2}} \quad (25)$$

where $\mathbf{T} \geqslant 0$ is the solution to the Lyapunov equation

$$\mathbf{A}_{\text{cl}}^{\text{T}}\mathbf{T} + \mathbf{T}\mathbf{A}_{\text{cl}} + \mathbf{C}^{\text{T}}\mathbf{C} = \mathbf{0} \quad (26)$$

then equation (24) is asymptotically stable. A proof of this result is given in the appendix.

Finally, we note that, because statistical linearization is merely an approximation of the true system dynamics, it is important that certain precautions be taken to ensure that a stable covariance matrix is indeed a justifiable approximation of the true mean-square system behavior. At the bare minimum, it should be ensured that the true system is bounded-input bounded-state stable, in order for the approximate ensemble averages to be meaningful. For the type of nonlinear system we consider here (i.e., where the nonlinearities arise due to Coulomb friction), this may be done by checking that the matrix $\mathbf{A} + \mathbf{B}\mathbf{K}$ is asymptotically stable. It is a straightforward Lyapunov analysis to show that if this condition holds, then the ratio $\|\mathbf{x}_{\text{h}}\|_{\infty}/\|a\|_{\infty}$ is always

bounded, independently of the amount of Coulomb friction present in the system.

4.2. Stationary optimal energy harvesting

Recall that the energy harvesting objective is to maximize the average power generated in stationarity; i.e.,

$$\bar{P}_{\text{gen}} = -\text{tr}\{[\tfrac{1}{2}\mathbf{K}^{\text{T}}\mathbf{B}^{\text{T}} + \tfrac{1}{2}\mathbf{B}\mathbf{K} + R\mathbf{K}^{\text{T}}\mathbf{K}]\mathbf{S}\} \quad (27)$$

over the feedback gain matrix $\mathbf{K}$. Since this optimization is subject to the constraint in to equation (23), we define the Hamiltonian $\mathcal{H}$ as

$$\mathcal{H} = -\bar{P}_{\text{gen}} + \text{tr}\{\mathbf{P}(\mathbf{A}_{\text{cl}}\mathbf{S} + \mathbf{S}\mathbf{A}_{\text{cl}}^{\text{T}} + \mathbf{G}\mathbf{G}^{\text{T}})\} \quad (28)$$

where $\mathbf{P} = \mathbf{P}^{\text{T}}$ is a Lagrange multiplier matrix which enforces the stationary solution to equation (23) as a constraint in the optimization. Thus, we have the following minimax problem

$$\mathbf{K} = \underset{\mathbf{K}}{\text{argmin}}\left[\min_{\mathbf{S}=\mathbf{S}^{\text{T}}} \max_{\mathbf{P}=\mathbf{P}^{\text{T}}} \mathcal{H}\right]. \quad (29)$$

To find the optimal solution to the problem in equation (29), we take the partial derivative of the Hamiltonian with respect to each of the decision variables and set these quantities equal to zero. This procedure constitutes a standard approach to solving an optimal control problem [28]. For brevity, we suppress the intermediate steps required to compute the partial derivatives and merely highlight their final analytical expressions. We start by taking the partial derivative of $\mathcal{H}$ with respect to $\mathbf{S}$; i.e.,

$$\frac{\partial\mathcal{H}}{\partial\mathbf{S}} = \frac{1}{2}\mathbf{K}^{\text{T}}\mathbf{B}^{\text{T}} + \frac{1}{2}\mathbf{B}\mathbf{K} + R\mathbf{K}^{\text{T}}\mathbf{K} + \mathbf{P}\mathbf{A}_{\text{cl}}$$
$$+ \mathbf{A}_{\text{cl}}^{\text{T}}\mathbf{P} - \mathbf{U}\mathbf{P}\mathbf{V} - \mathbf{V}^{\text{T}}\mathbf{P}\mathbf{U}^{\text{T}} = \mathbf{0} \quad (30)$$

where $\mathbf{V} = \mathbf{V}(t)|_{\Sigma(t)=\mathbf{S}}$ and

$$\mathbf{U} = \frac{1}{2}\frac{\mathbf{C}^{\text{T}}\mathbf{C}\mathbf{S}}{\mathbf{C}\mathbf{S}\mathbf{C}^{\text{T}}}. \quad (31)$$

Next, we take the partial derivative of $\mathcal{H}$ with respect to $\mathbf{K}$; i.e.,

$$\frac{\partial\mathcal{H}}{\partial\mathbf{K}} = \mathbf{S}\mathbf{B}^{\text{T}} + 2R\mathbf{S}\mathbf{K}^{\text{T}} + 2\mathbf{S}\mathbf{P}\mathbf{B} = \mathbf{0}. \quad (32)$$

Pre-multiplying equation (32) by $\mathbf{S}^{-1}$ and solving for $\mathbf{K}$ results in equation (8), but with the new $\mathbf{P}$ found via equation (30) rather than the Riccati equation in equation (9). It is not necessary to take the partial derivative of $\mathcal{H}$ with respect to the Lagrange multiplier $\mathbf{P}$ as this will just give us back the equilibrium condition for $\mathbf{S}$ in equation (23). Finally, we can substitute equation (8) into (23) and (30) to arrive at two coupled, nonlinear algebraic equations for $\mathbf{S}$ and $\mathbf{P}$ that must hold at the optimum; i.e.,

$$\left[\mathbf{A} + \mathbf{V} - \frac{1}{R}\mathbf{B}\mathbf{B}^{\text{T}}\left(\mathbf{P} + \frac{1}{2}\mathbf{I}\right)\right]\mathbf{S}$$
$$+ \mathbf{S}\left[\mathbf{A} + \mathbf{V} - \frac{1}{R}\mathbf{B}\mathbf{B}^{\text{T}}\left(\mathbf{P} + \frac{1}{2}\mathbf{I}\right)\right]^{\text{T}} + \mathbf{G}\mathbf{G}^{\text{T}} = \mathbf{0} \quad (33)$$

$$[\mathbf{A} + \mathbf{V}]^T\mathbf{P} + \mathbf{P}[\mathbf{A} + \mathbf{V}] - \frac{1}{R}\left(\mathbf{P} + \frac{1}{2}\mathbf{I}\right)\mathbf{BB}^T\left(\mathbf{P} + \frac{1}{2}\mathbf{I}\right)$$

$$- \mathbf{UPV} - \mathbf{V}^T\mathbf{PU}^T = \mathbf{0}. \tag{34}$$

4.3. Iterative algorithm

Because $\mathbf{U}$ and $\mathbf{V}$ depend on $\mathbf{S}$, equations (33) and (34) are coupled nonlinear algebraic equations. As such, solutions for the stationary covariance matrix $\mathbf{S}$ and the Lagrange multiplier $\mathbf{P}$ must be computed iteratively. To do this, we begin by linearizing equation (28) about $\mathbf{S} = \mathbf{S}_0$; i.e.,

$$\tilde{\mathcal{H}} = -\bar{P}_{\text{gen}} + \text{tr}\Bigg\{\mathbf{P}\Bigg[[\mathbf{A} + \mathbf{BK} + \mathbf{V}_0]\mathbf{S}$$
$$+ \mathbf{S}[\mathbf{A} + \mathbf{BK} + \mathbf{V}_0] + \mathbf{GG}^T$$
$$+ \frac{1}{2}(\mathbf{V}_0\mathbf{S}_0 + \mathbf{S}_0\mathbf{V}_0^T)\left(1 - \frac{\mathbf{CSC}^T}{\mathbf{CS}_0\mathbf{C}^T}\right)\Bigg]\Bigg\} \tag{35}$$

where $\mathbf{V}_0 = \mathbf{V}|_{\mathbf{S}=\mathbf{S}_0}$. Regrouping terms, we have that

$$\tilde{\mathcal{H}} = \text{tr}\{\mathbf{P}[\mathbf{GG}^T + \frac{1}{2}(\mathbf{V}_0\mathbf{S}_0 + \mathbf{S}_0\mathbf{V}_0^T)]$$
$$+ \mathbf{S}[\frac{1}{2}\mathbf{K}^T\mathbf{B}^T + \frac{1}{2}\mathbf{BK} + R\mathbf{K}^T\mathbf{K}$$
$$+ \mathbf{P}[\mathbf{A} + \mathbf{BK} + \mathbf{V}_0] + [\mathbf{A} + \mathbf{BK} + \mathbf{V}_0]^T\mathbf{P}$$
$$- \mathbf{U}_0\mathbf{PV}_0 - \mathbf{V}_0^T\mathbf{PU}_0^T]\} \tag{36}$$

where $\mathbf{U}_0 = \mathbf{U}|_{\mathbf{S}=\mathbf{S}_0}$. If $\{\mathbf{K}, \mathbf{P}, \mathbf{S}\}$ are the optimal parameters for original problem, they will also be optimal parameters for the linearized problem with $\mathbf{S}_0$ equal to its optimal value.

Now, consider that if we assume that the optimal $\mathbf{K}$ is such that $\mathbf{A}_{\text{cl}}$ is asymptotically stable, then $\mathbf{S}_0 > 0$ can be assumed to hold at the optimal solution as well. If this is the case then, using the linearized Hamiltonian and substituting the optimal relationship between $\mathbf{K}$ and $\mathbf{P}$ in equation (8), the value of $\tilde{\mathcal{H}}$ is bounded by

$$\tilde{\mathcal{H}} > \text{tr}\{\mathbf{P}[\mathbf{GG}^T + \frac{1}{2}(\mathbf{V}_0\mathbf{S}_0 + \mathbf{S}_0\mathbf{V}_0^T)]\} \tag{37}$$

where $\mathbf{P}$ is subject to the constraint

$$[\mathbf{A} + \mathbf{V}_0]^T\mathbf{P} + \mathbf{P}[\mathbf{A} + \mathbf{V}_0] - \frac{1}{R}\left(\mathbf{P} + \frac{1}{2}\mathbf{I}\right)\mathbf{BB}^T\left(\mathbf{P} + \frac{1}{2}\mathbf{I}\right)$$

$$- \mathbf{U}_0\mathbf{PV}_0 - \mathbf{V}_0^T\mathbf{PU}_0^T > 0. \tag{38}$$

Furthermore, we know from equation (34) that for any optimal solution, equation (38) holds with an equality. But if this is true, then equation (37) also holds with an equality at any optimum. Thus, for $\mathbf{S}_0 > 0$ equal to the optimal $\mathbf{S}$, the optimization

$$\mathbf{P} = \underset{\mathbf{P}}{\text{argmax}}\,\text{tr}\{\mathbf{P}[\mathbf{GG}^T + \frac{1}{2}(\mathbf{V}_0\mathbf{S}_0 + \mathbf{S}_0\mathbf{V}_0^T)]\} \tag{39}$$

subject to equation (38), or equivalently, the LMI

$$\begin{bmatrix} [\mathbf{A} + \mathbf{V}_0]^T\mathbf{P} + \mathbf{P}[\mathbf{A} + \mathbf{V}_0] - \mathbf{U}_0\mathbf{PV}_0 - \mathbf{V}_0^T\mathbf{PU}_0^T & \left(\mathbf{P} + \frac{1}{2}\mathbf{I}\right)\mathbf{B} \\ \mathbf{B}^T\left(\mathbf{P} + \frac{1}{2}\mathbf{I}\right) & R \end{bmatrix} > 0 \tag{40}$$

will give the same optimal solution for $\mathbf{P}$.

Motivated by the above, we define the matrix function $\mathbf{P} = \Theta(\mathbf{S}_0)$, over the domain $\mathbf{S}_0 > 0$, as

$$\Theta(\mathbf{S}_0) =$$

$$\underset{\mathbf{P}}{\text{sol}}\begin{cases} \text{Given}: & \mathbf{S}_0 > 0 \\ \text{Maximize}: & \text{tr}\{\mathbf{P}[\mathbf{GG}^T + \frac{1}{2}(\mathbf{V}_0\mathbf{S}_0 + \mathbf{S}_0\mathbf{V}_0^T)]\} \\ \text{Over}: & \mathbf{P} \\ \text{Subject to}: & \text{LMI constraint in equation (40).} \end{cases}$$

$$\tag{41}$$

The optimization in equation (41) is convex and is feasible for any $\mathbf{S}_0 > 0$, and may therefore be viewed as a unique function over the domain $\mathbf{S}_0 > 0$. Using this function, the following iterative algorithm can be used to solve for the values of $\mathbf{S}$ and $\mathbf{P}$ at the optimum:

Step 0. Initialize $\mathbf{S}_0$ by solving the linear energy harvesting problem (i.e., with $\mathbf{U} = \mathbf{V} = \mathbf{0}$).
Step 1. Compute new values for $\mathbf{V}_0$ and $\mathbf{U}_0$ using $\mathbf{S}_0$.
Step 2. Compute $\mathbf{P} = \Theta(\mathbf{S}_0)$.
Step 3. In equation (33), fix $\mathbf{V} \leftarrow \mathbf{V}_0$ and solve the resultant Lyapunov equation for $\mathbf{S}$.
Step 4. Set $\mathbf{S}_0 \leftarrow \mathbf{S}$ and return to Step 1.

Convergence of the algorithm is reached when the absolute value of the change in $\bar{P}_{\text{gen}}$ between the current and previous iteration is below a certain tolerance. The value of $\bar{P}_{\text{gen}}$ at the first iteration can be calculated using equation (10) while the value of $\bar{P}_{\text{gen}}$ at any subsequent iteration can be calculated using equation (27).

Here, we make no claim that this algorithm always converges, although it did converge for all examples considered in this paper. Once convergence is reached, asymptotic stability of $\mathbf{A}_{\text{cl}}$ at the optimum should be verified. Furthermore, it should also be verified that the matrix $\mathbf{A} + \mathbf{BK}$ is asymptotically stable, and that inequality equation (25) holds. All conditions were found to hold uniformly in the solutions for the examples considered here.

For the energy harvesting example considered in this paper, the above algorithm was found to converge within 10–20 iterations. Using the system defined in equation (6), we illustrate the convergence of the proposed algorithm in figure 3. For this example, we fix $R = 5\ \Omega$ and $\zeta_a = 0.5$ and run the algorithm with a convergence tolerance of $1e^{-6}$. As shown, the algorithm converges to $\bar{P}_{\text{gen}} = 10.1$ W in 14 iterations.

4.4. Example

We can gain some valuable insight into the statistically linearized energy harvesting problem by comparing the $\bar{P}_{\text{gen}}$ resulting from the optimal static admittance with the $\bar{P}_{\text{gen}}$ resulting from the optimal feedback control law. The plots in figure 4 illustrate this comparison for the SDOF energy harvester characterized by equation (6). We see that the curves in both plots monotonically decrease as ζ_a increases and that the curves in figure 4(b) have higher $\bar{P}_{\text{gen}}$ values than the curves in figure 4(a).
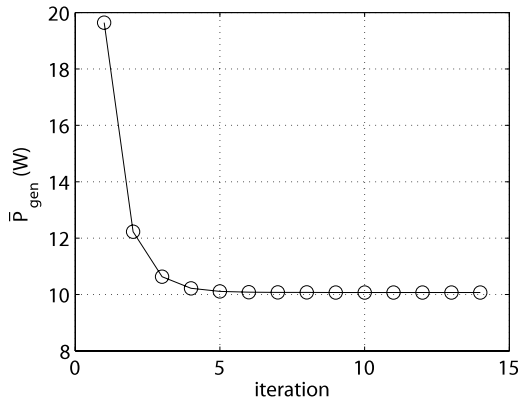
Figure 3. Example of the iterative algorithm converging for $R = 5\ \Omega$ and $\zeta_a = 0.5$.
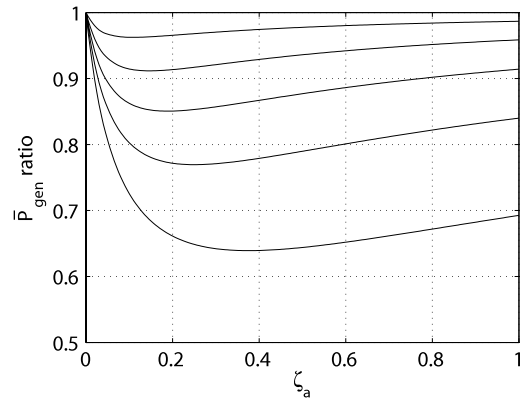
Figure 5. $\bar{P}_{gen}$ ratio for R values of 2, 5, 10, 20, and 50 Ω (from bottom to top).

To illustrate the improvement in performance that can be achieved by implementing the feedback controller, we define the '$\bar{P}_{gen}$ ratio' in figure 5 as the ratio of $\bar{P}_{gen}$ resulting from the static admittance over $\bar{P}_{gen}$ resulting from the feedback controller. From this plot, we obtain the interesting result that there is a finite bandwidth for $a(t)$ at which the feedback controller is most beneficial. Another important result of this analysis can be seen in the narrowband limit as $\zeta_a \to 0$. At this limit, we see that the $\bar{P}_{gen}$ ratio is equal to unity. As pointed out in [29] (for the case without Coulomb friction), this is due to the fact that the velocity and acceleration gains are the only gains in **K** required for the optimal feedback controller. In the narrowband limit, $\dot{r}(t)$ and $a(t)$ become purely sinusoidal and exactly in phase, which means that knowledge of both is redundant. Thus, we can conclude that for the case where Coulomb friction is included in the dynamics of the harvester, that the optimal $i(t)$ is attained by imposing a static admittance.

Finally, we illustrate the effect that Coulomb friction has on the average power generated in figure 6. The 'friction ratio' curves in this plot are defined as the ratio of $\bar{P}_{gen}$ resulting from the statistically linearized feedback controller over $\bar{P}_{gen}$ resulting from the feedback controller without Coulomb
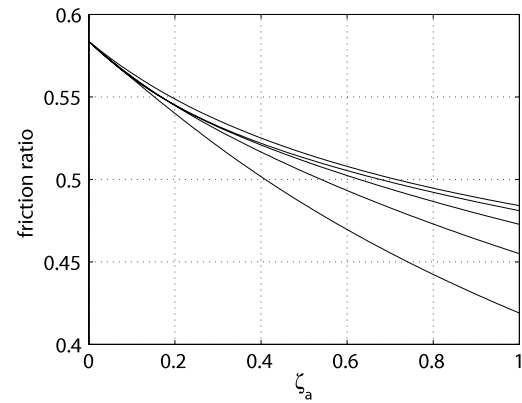
Figure 6. Friction performance ratio for R values of 2, 5, 10, 20, and 50 Ω (from top to bottom).

friction. As shown, the ratios decrease as ζ_a increases for all values of resistive losses. In addition, we see that in the limit as $\zeta_a \to 0$, the ratios approach the same value which is independent of R. From this analysis, we can conclude that systems with higher resistive losses are more sensitive (in terms of performance) to the effects of Coulomb friction when the system is excited by broadband disturbances.
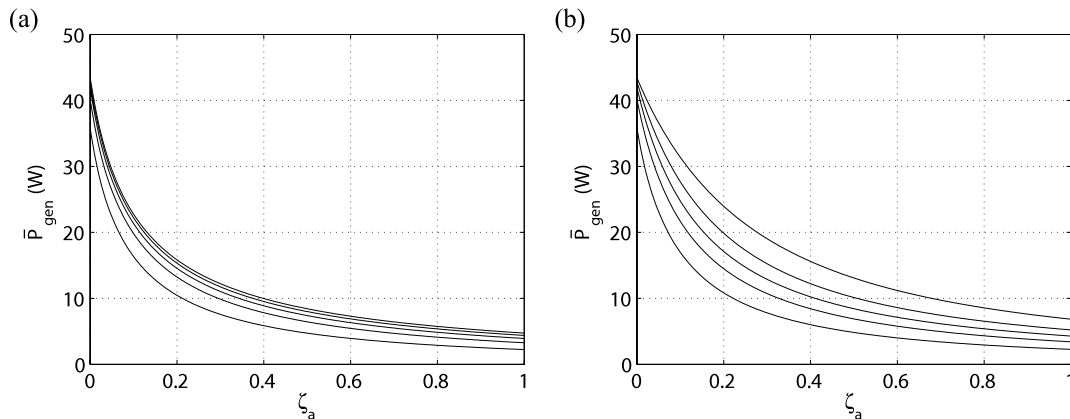
Figure 4. Comparison of the average power generated by: (a) the optimal static admittance and; (b) the optimal feedback control law; for R values of 2, 5, 10, 20, and 50 Ω (from top to bottom).
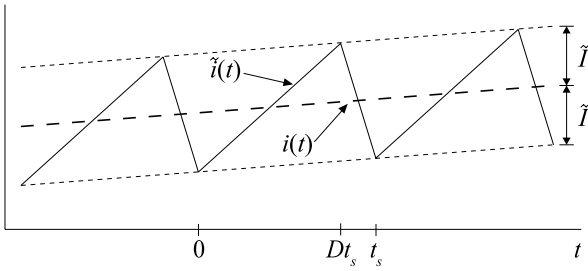
Figure 7. Transducer current with the electronics operating in CCM.

5. Non-quadratic loss model

5.1. Loss model of an H-bridge in CCM

Consider again the H-bridge in figure 2(a). In this circuit, each MOSFET/diode pair is operated like a power electronic switch. For this paper, we consider the operation of this system in bi-directional continuous conduction mode (CCM). In this operating regime, the transducer's current is controlled to take on the shape shown in figure 7. As shown, current from the transducer is controlled to be a triangle wave, which is triggered by a switching clock with period t_s. The switching frequency $f_s = 1/t_s$ is presumed to be at least a decade above the pre-dominant dynamics of the harvester (i.e., $f_s > 10\omega_a/2\pi$), and as such, the high-frequency component of the current is filtered out by the inertia of the transducer. Consequently, it is only the low-frequency switch-averaged current that significantly influences the overall system response. For clarity, we refer to $i(t)$ and $v(t)$ as the switch-averaged current and voltage, respectively, and $\tilde{i}(t)$ and $\tilde{v}(t)$ as the actual current and voltage, respectively, with the high-frequency content included.

For the analysis of the H-bridge presented here, we assume that $\tilde{i}(t) > 0$ for $t \in [0, t_s]$. Making the assumption that $\tilde{i}(t) < 0$ for $t \in [0, t_s]$ would result in the same expression for the losses. As such, the H-bridge operated in CCM works as follows. At the leading edge of each switching cycle, MOSFETs Q_1 and Q_4 are gated on for the first Dt_s seconds, which increases $\tilde{i}(t)$. The equivalent circuit made by this current path can be seen in figure 8(a). Then, at time $t = Dt_s$, the conducting MOSFETs Q_1 and Q_4 are gated off, causing the free-wheeling diodes Q_2 and Q_3 to conduct. This causes $\tilde{i}(t)$ to decrease until the switching period t_s is reached. The

equivalent circuit made by this current path can be seen in figure 8(b).

The power dissipated during this process is what is known as conductive dissipation. We assume this dissipation to be a consequence of forward conduction losses in the MOSFETs and diodes. These two devices have very different dissipative characteristics, which are nonlinear. To simplify the analysis, we make the conservative assumption that energy is dissipated like a diode in series with a resistor over the entire switching period. We define the total forward conduction voltage of the diodes as V_d and the total resistance of the conducting MOSFETs in series with the equivalent resistance of transducer's coil as R_m. Additional losses, such as transition and gating losses in the MOSFETs, are neglected in this analysis as they will have a negligible effect on the loss model for the levels of power considered in this paper. However, for piezoelectric energy harvesting applications, where the levels of power are on the order of μW–mW, transition and gating losses will have a much greater effect on the efficiency of the electronics and they should be in included in the loss model. See [13] for an analysis which includes these losses.

The goal is to determine an expression for the losses in the H-bridge in terms of $i(t)$ and the non-dynamic parameters of the drive. We begin by following Kirchoff's voltage law in the direction of positive current for the circuits in figure 8. Thus, we have that the voltage across the inductor is

$$v_L(t) = \begin{cases} V_S - \tilde{v}(t) - V_d - R_m\tilde{i}(t) : & t \in [0, Dt_s] \\ -V_S - \tilde{v}(t) - V_d - R_m\tilde{i}(t) : & t \in [Dt_s, t_s]. \end{cases}$$
(42)

Next, we make the assumption that the current ripple on the inductor is small (i.e., $|i(t)| \gg \tilde{I}$ in figure 7) during steady-state operation of the drive. As such, we temporarily approximate $\tilde{i}(t)$ and $\tilde{v}(t)$ as being constant over one switching period t_s (i.e., $\tilde{i}(t) \approx i$ and $\tilde{v}(t) \approx v$). Then we have that the average value of the voltage across the inductor, $\bar{v}_L$, during each switching cycle is equal to 0; i.e.,

$$\bar{v}_L = \frac{1}{t_s} \int_0^{t_s} v_L(t) \, dt \approx Dt_s(V_S - v - V_d - R_m i)$$
$$+ (1 - D)t_s(-V_S - v - V_d - R_m i) = 0. \quad (43)$$

The approximation in equation (43), referred to 'inductor volt-second balance', constitutes a standard approach for analyzing power electronic converters that are operating in

(a)

(b)
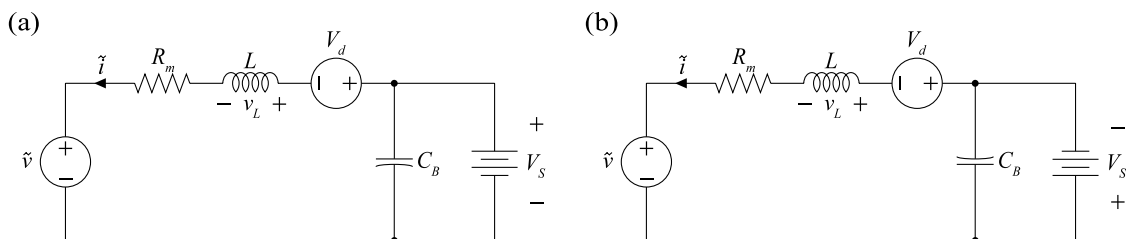
Figure 8. Equivalent circuit made by the H-bridge and transducer for (a) $t \in [0, Dt_s]$ and (b) $t \in [Dt_s, t_s]$.

CCM [30]. From equation (43), we can then solve for the value of the steady-state duty cycle D as

$$D = \frac{V_S + v + V_d + R_m i}{2V_S}. \tag{44}$$

The power dissipated in the electronics over the course of a switching cycle, $P_d(i)$, can be computed by integrating the total resistive losses and the total diode losses over the switching period t_s; i.e.,

$$P_d(i) = \frac{1}{t_s}\left\{\int_0^{t_s} R_m \tilde{i}^2(t)\, dt + \int_0^{t_s} V_d|\tilde{i}(t)|\, dt\right\} \tag{45}$$

$$= R_m(i^2(t) + \tfrac{1}{3}\tilde{I}^2) + V_d|i(t)|. \tag{46}$$

where equation (46) assumes the triangular current waveform in figure 7. We can derive an expression for the magnitude of the current ripple using the expression for the inductor voltage during the interval $t \in [0, Dt_s]$; i.e.,

$$\tilde{I} = \frac{Dt_s}{2L}v_L(t) = \frac{t_s}{2L}\frac{V_S^2 - (v + V_d + R_m i)^2}{2V_S}. \tag{47}$$

We can conservatively approximate the magnitude of the current ripple by assuming that $V_S \gg v + V_d + R_m i$. Thus, we have that the upper bound for $\tilde{I}$ is

$$\tilde{I} = \frac{V_S}{4Lf_s} \tag{48}$$

and the expression for power dissipation in the electronics is conservatively approximated by

$$P_d(i) = \frac{R_m V_S^2}{48L^2 f_s^2} + R_m i^2(t) + V_d|i(t)|. \tag{49}$$

5.2. Statistically linearized energy harvesting with non-quadratic loss models

We now propose a technique for expanding the theory presented in section 4 to accommodate non-quadratic loss models. If the dynamics of the closed-loop system are statistically linearized, then the response distribution for the augmented system state $\mathbf{x}(t)$ is assumed to be Gaussian. Consequently, the distribution of the current $i(t)$ is also Gaussian, with zero mean and variance $s_i = \mathcal{E}\, i^2(t)$. We may evaluate the average power dissipation by taking the expectation of equation (49); i.e.,

$$\bar{P}_d = \mathcal{E}\, P_d(i)$$

$$= \frac{1}{\sqrt{2\pi s_i}}\int_{-\infty}^{\infty} \exp\{-i^2(t)/2s_i\}P_d(i)\, di(t) \tag{50}$$

$$= \frac{R_m V_S^2}{48L^2 f_s^2} + R_m s_i + \left(V_d\sqrt{\frac{2}{\pi}}\right)s_i^{1/2}. \tag{51}$$

Next, we note that if $\bar{P}_d$ is semiconcave, i.e., if

$$\frac{\partial^2 \bar{P}_d}{\partial s_i^2} \leqslant 0, \qquad \forall s_i > 0 \tag{52}$$

then it follows that $\bar{P}_d$ can be overbounded by its first-order Taylor expansion about any positive variance s_i^0; i.e.,

$$\bar{P}_d \leq \bar{P}_d^0 + R^0 s_i \tag{53}$$

where

$$R^0 = \left.\frac{\partial \bar{P}_d}{\partial s_i}\right|_{s_i=s_i^0} \tag{54}$$

$$\bar{P}_d^0 = \bar{P}_d|_{s_i=s_i^0} - R^0 s_i^0 \tag{55}$$

with the equality holding (as well as the slope) where $s_i = s_i^0$. The loss model derived in equation (51) is semiconcave because both terms involving s_i have exponents less than or equal to 1.

For semiconcave loss models, we may conservatively overbound the losses through a summation of a static (i.e., current-independent) loss model and a quadratic (i.e., resistive) loss model. This permits us to nest the above loss model inside the iterative algorithm used to solve equation (41) as follows:

Step 0. Initialize the loss model by taking an arbitrary value for $R > 0$ and initialize $\mathbf{S}_0$ by solving the linear energy harvesting problem (i.e., with $\mathbf{U} = \mathbf{V} = \mathbf{0}$).
Step 1. Compute new values for $\mathbf{V}_0$ and $\mathbf{U}_0$ using $\mathbf{S}_0$.
Step 2. Compute $\mathbf{P} = \Theta(\mathbf{S}_0)$.
Step 3. Compute $\mathbf{K}$ from equation (8) and fix $\mathbf{V} \leftarrow \mathbf{V}_0$ in equation (33) to solve the resultant Lyapunov equation for $\mathbf{S}$.
Step 4. Compute the variance of the current, as $s_i^0 = \mathbf{KSK}^T$.
Step 5. For the new value of s_i^0, compute R^0 via equation (54).
Step 6. Set $R \leftarrow R^0$ and $\mathbf{S}_0 \leftarrow \mathbf{S}$ and return to Step 1.

Convergence of the algorithm is reached when the absolute value of the change in $\bar{P}_{gen}$ between the current and previous iteration is below a certain tolerance. The value of $\bar{P}_{gen}$ at the first iteration can be calculated using equation (10) while the value of $\bar{P}_{gen}$ at any subsequent iteration can be calculated by

$$\bar{P}_{gen} = -\text{tr}\{[\tfrac{1}{2}\mathbf{K}^T\mathbf{B}^T + \tfrac{1}{2}\mathbf{BK} + R^0\mathbf{K}^T\mathbf{K}]\mathbf{S}\} - \bar{P}_d^0. \tag{56}$$

5.3. Example

To illustrate how the non-quadratic loss model effects the average power generated, we return to the SDOF energy harvester system described in equation (6). The parameters in

Table 2. H-bridge electronic parameters for the loss model.

Parameter	Value
R_m	2.61 Ω
V_d	1.4 V
L	8.93 mH
f_s	33 kHz
V_S	80 V
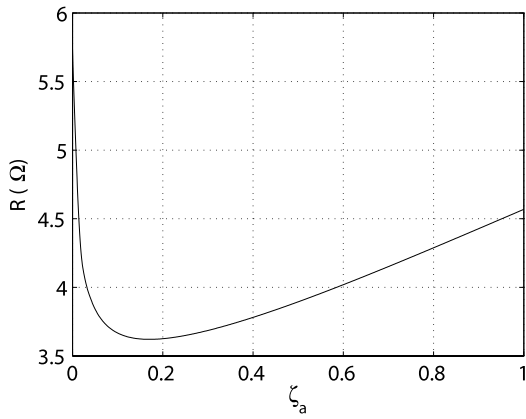
Figure 9. Plot of the equivalent resistive losses R versus ζ_a.

are switching at a frequency of 33 kHz. This is the switching frequency for a S16A8 servo drive from Advanced Motion Controls [31] used in the experimental validation of the transducer in [9].

We begin by illustrating the equivalent resistive losses resulting from the non-quadratic loss model in equation (49) over a range of disturbance bandwidths. The plot in figure 9 shows the dependence of R on ζ_a for $\zeta_a \in [0, 1]$. From this plot we see that R initially decreases as ζ_a increases until it reaches a minimum value. In this case the minimum value is $R = 3.62$ Ω, which occurs at $\zeta_a = 0.164$. Once R reaches this minimum value it then increases linearly as ζ_a increases. This relationship suggests that there is a specific disturbance bandwidth where the electronics are operating most efficiently.

Next, we illustrate how both the Coulomb friction in the electromagnetic transducer and the conduction voltage of the diodes in the H-bridge influences the performance of the energy harvesting system. As such, we plot the $\bar{P}_{gen}$ surface for various combinations of $\{F_c, V_d\}$ and for three disturbance bandwidth values. The plots in figures 10(a)–(c) illustrate the $\bar{P}_{gen}$ surface for ζ_a values of 0.05, 0.2, and 0.7, respectively. From these plots we see that as F_c and V_d approach 0, the value obtained for $\bar{P}_{gen}$ approaches the performance from the linear energy harvesting example with purely resistive losses. In addition, we see that $\bar{P}_{gen}$ becomes more sensitive to increases F_c and V_d as ζ_a increases.

If either V_d or F_c is sufficiently large, power generation will effectively become infeasible, and $\bar{P}_{gen} \approx 0$ at the

the loss model are listed in table 2 and we justify these values as follows. We assume that the diodes are standard silicon with each modeled as possessing a current-independent conduction voltage of 0.7 V. The MOSFETs have a drain-to-source impedance which is resistive, with a value of 0.1 Ω when gated with a gate–source voltage of 1.5 V. For the inductor, we take its inductance to be that of winding of the transducer's coil (i.e., $L = 8.93$ mH). In addition, we know that winding of the coil has an effective series resistance of 2.41 Ω. Thus, the total conductive loss parameters for the H-bridge are taken to be $V_d = 2 \times 0.7 = 1.4$ V and $R_m = 2 \times 0.1 + 2.41 = 2.61$ Ω. Finally, we assume that the H-bridge is connected to a constant 80 V DC voltage source and that the MOSFETs

Figure 10. Surface plots for $\bar{P}_{gen}$ as a function of $\{F_c, V_d\}$ for: (a) $\zeta_a = 0.05$; (b) $\zeta_a = 0.2$; and (c) $\zeta_a = 0.7$.
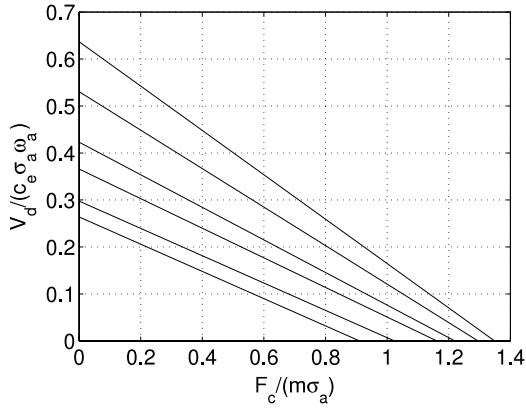
Figure 11. Plot of the nondimensional Coulomb friction and diode conduction voltage that results in $\bar{P}_{\text{gen}} \approx 0$, for ζ_a values of 0.05, 0.1, 0.2, 0.3, 0.5, 0.7 (from top to bottom).

optimum. Levels of $\{V_d, F_c\}$ resulting in this condition are illustrated in figure 11. In this plot, both F_c and V_d are nondimensionalized by using the standard deviation of the disturbance acceleration σ_a. Furthermore, each of the lines in the plot correspond to a different disturbance bandwidths ζ_a. If the values of F_c and V_d (for a given σ_a and ζ_a) results in a point that is at or above its corresponding line, then $\bar{P}_{\text{gen}} \approx 0$. Similarly, if the values of F_c and V_d (for a given σ_a and ζ_a) results in a point that is below its corresponding line, then $\bar{P}_{\text{gen}} > 0$. From the plot, we see that the levels of V_d and F_c required for significant power generation are heavily coupled, and thus cannot be considered in isolation.

6. Conclusions

In order to fully maximize the potential power generation from an actively controlled vibratory energy harvester, the mechanical and electrical nonlinearities in the system must be accounted for in the control design. Nonlinearities arising in the dynamics of the vibratory system can be statistically linearized if the system is excited by a stochastic disturbance and its response is approximated by a Gaussian distribution. This paper illustrates how to account for the Coulomb friction present in a stochastically excited SDOF oscillator and maximize the average power generation by simultaneously solving two coupled nonlinear algebraic equations. These equations are derived from first principles and an iterative algorithm is proposed to solve for the statistically linearized covariance matrix as well as the optimal feedback gain matrix. For the statistically linearized energy harvesting system with purely resistive losses, it is shown that the full-state feedback controller generates the same amount of average power as the static admittance for a narrowband disturbance.

Additionally, this paper presents a nonlinear loss model for the conductive power dissipated in an H-bridge that is operated in CCM. As such, the proposed statistical linearization and optimal control algorithm is augmented to include the non-quadratic loss model. However, the convergence of the algorithm is only guaranteed if the loss model exhibits the semiconcave property, and this property

may not hold for all systems. For an H-bridge operating in CCM, we illustrate that the equivalent resistance resulting from the non-quadratic loss model reaches a minimum value at a nontrivial disturbance bandwidth. In addition, for a given disturbance bandwidth, we show the influence of varying levels of Coulomb friction and diode conduction voltage on the performance of the energy harvesting system. Finally, we illustrate that there are critical levels of Coulomb friction and diode conduction voltage beyond which power generation becomes infeasible, and that the critical values of these two quantities are strongly coupled.

Acknowledgments

Appendix

Proof of the stability condition in equation (25):

If equation (24) is unstable, this implies the existence of an eigenvalue $\lambda > 0$, and a corresponding eigenvector $\mathbf{S}_u \neq 0$, such that

$$\lambda \mathbf{S}_u = \mathbf{A}_{cl}\mathbf{S}_u + \mathbf{S}_u\mathbf{A}_{cl}^T - \sqrt{\frac{1}{2\pi}}\frac{\mathbf{C}\mathbf{S}_u\mathbf{C}^T}{(\mathbf{C}\mathbf{S}\mathbf{C}^T)^{3/2}}[\mathbf{F}\mathbf{C}\mathbf{S} + \mathbf{S}\mathbf{C}^T\mathbf{F}^T]. \quad (57)$$

Because we assume take asymptotic stability of $\mathbf{A}_{cl}$ for granted, the solution $\mathbf{S}_u$ to the above satisfies

$$\mathbf{S}_u = \int_0^\infty \exp[(\mathbf{A}_{cl} - \tfrac{1}{2}\lambda\mathbf{I})t]$$
$$\times \left[-\sqrt{\frac{1}{2\pi}}\frac{\mathbf{C}\mathbf{S}_u\mathbf{C}^T}{(\mathbf{C}\mathbf{S}\mathbf{C}^T)^{3/2}}[\mathbf{F}\mathbf{C}\mathbf{S} + \mathbf{S}\mathbf{C}^T\mathbf{F}^T] \right]$$
$$\times \exp[(\mathbf{A}_{cl}^T - \tfrac{1}{2}\lambda\mathbf{I})t]\,\mathrm{d}t \quad (58)$$
$$= -\sqrt{\frac{1}{2\pi}}\frac{\mathbf{C}\mathbf{S}_u\mathbf{C}^T}{(\mathbf{C}\mathbf{S}\mathbf{C}^T)^{3/2}}\int_0^\infty \exp[\mathbf{A}_{cl}t][\mathbf{F}\mathbf{C}\mathbf{S} + \mathbf{S}\mathbf{C}^T\mathbf{F}^T]$$
$$\times \exp[\mathbf{A}_{cl}^T t]\mathrm{e}^{-\lambda t}\,\mathrm{d}t \quad (59)$$
$$= -\sqrt{\frac{1}{2\pi}}\frac{\mathbf{C}\mathbf{S}_u\mathbf{C}^T}{(\mathbf{C}\mathbf{S}\mathbf{C}^T)^{3/2}}\mathbf{W} \quad (60)$$

where $\mathbf{W}$ is the solution to the Lyapunov equation

$$\mathbf{A}_{cl}\mathbf{W} + \mathbf{W}\mathbf{A}_{cl}^T - \lambda\mathbf{W} + \mathbf{F}\mathbf{C}\mathbf{S} + \mathbf{S}\mathbf{C}^T\mathbf{F}^T = \mathbf{0}. \quad (61)$$

Consequently, we have that

$$\mathbf{C}\mathbf{S}_u\mathbf{C}^T = -\sqrt{\frac{1}{2\pi}}\frac{\mathbf{C}\mathbf{S}_u\mathbf{C}^T}{(\mathbf{C}\mathbf{S}\mathbf{C}^T)^{3/2}}\mathbf{C}\mathbf{W}\mathbf{C}^T \quad (62)$$

or, rearranging,

$$\mathbf{C}\mathbf{S}_u\mathbf{C}^T\left(1 + \sqrt{\frac{1}{2\pi}}\frac{\mathbf{C}\mathbf{W}\mathbf{C}^T}{(\mathbf{C}\mathbf{S}\mathbf{C}^T)^{3/2}}\right) = 0. \quad (63)$$

Through duality, this is equivalent to

$$\mathbf{CS}_u\mathbf{C}^T\left(1 + \sqrt{\frac{2}{\pi}}\frac{\operatorname{tr}[\mathbf{FCST}_\lambda]}{(\mathbf{CSC}^T)^{3/2}}\right) = 0 \qquad (64)$$

where $\mathbf{T}_\lambda$ is the solution to

$$\mathbf{A}_{cl}^T\mathbf{T}_\lambda + \mathbf{T}_\lambda\mathbf{A}_{cl} - \lambda\mathbf{T}_\lambda + \mathbf{C}^T\mathbf{C} = \mathbf{0}. \qquad (65)$$

We know $\mathbf{T}_\lambda \geqslant 0$ because $\mathbf{C}^T\mathbf{C} \geqslant 0$ and $\mathbf{A}_{cl} - \frac{1}{2}\lambda\mathbf{I}$ is asymptotically stable for any $\lambda > 0$. Furthermore, we know that $\mathbf{T}_\lambda \to 0$ as $\lambda \to \infty$. Consequently, in equation (64), the solution $\mathbf{CS}_u\mathbf{C}^T = 0$ is unique for all $\lambda > 0$ if it can be shown that

$$\frac{|\operatorname{tr}[\mathbf{FCST}_\lambda]|}{(\mathbf{CSC}^T)^{3/2}} < \sqrt{\frac{\pi}{2}}, \qquad \forall \lambda > 0 \qquad (66)$$

because this implies that the multiplier in the parentheses in equation (64) can never be zero for $\lambda > 0$. But

$$|\operatorname{tr}[\mathbf{FCST}_\lambda]| = |\mathbf{CST}_\lambda\mathbf{F}| \qquad (67)$$

$$\leqslant (\mathbf{CST}_\lambda\mathbf{SC}^T)^{1/2}(\mathbf{F}^T\mathbf{T}_\lambda\mathbf{F})^{1/2} \qquad (68)$$

where we have used the observation that $\mathbf{T}_\lambda \geqslant 0$, and the Cauchy–Schwarz inequality. Thus, a conservative criterion for the uniqueness of the $\mathbf{CS}_u\mathbf{C}^T = 0$ solution is

$$\frac{(\mathbf{CST}_\lambda\mathbf{SC}^T)^{1/2}(\mathbf{F}^T\mathbf{T}_\lambda\mathbf{F})^{1/2}}{(\mathbf{CSC}^T)^{3/2}} < \sqrt{\frac{\pi}{2}}, \qquad \forall \lambda > 0. \qquad (69)$$

Now, we observe that because $\mathbf{T}_\lambda \geqslant 0$ and $\mathbf{A}_{cl}$ is stable, it is the case that if $\lambda_1 < \lambda_2$, then $\mathbf{T}_{\lambda_1} \geqslant \mathbf{T}_{\lambda_2}$. Consequently, the above bound is most tight at $\lambda = 0$, which gives the condition shown in equation (25). Assuming this condition is satisfied, the unstable eigenmode $\mathbf{S}_u$ must have $\mathbf{CS}_u\mathbf{C}^T = 0$. Thus, from equation (57), it must satisfy

$$[\mathbf{A}_{cl} - \tfrac{1}{2}\lambda\mathbf{I}]\mathbf{S}_u + \mathbf{S}_u[\mathbf{A}_{cl} - \tfrac{1}{2}\lambda\mathbf{I}]^T = \mathbf{0} \qquad (70)$$

which, because $\mathbf{A}_{cl} - \frac{1}{2}\lambda\mathbf{I}$ is asymptotically stable for all $\lambda > 0$, has the unique solution $\mathbf{S}_u = 0$. But $\mathbf{S}_u \neq 0$ in order to be an eigenmode, and thus we arrive at a contradiction. This completes the proof.

References

[1] Roundy S, Wright P K and Rabaey J 2002 A study of low level vibrations as a power source for wireless sensor nodes *J. Comput. Commun.* **26** 1131–44

[2] Anton S R and Sodano H A 2007 A review of power harvesting using piezoelectric materials (2003–2006) *Smart Mater. Struct.* **16** R1–21

[3] Knight C, Davidson J and Behrens S 2008 Energy options for wireless sensor nodes *Sensors* **8** 8037–66

[4] Zuo L, Scully B, Shestani J and Zhou Y 2010 Design and characterization of an electromagnetic energy harvester for vehicle suspensions *Smart Mater. Struct.* **19** 045003

[5] Nagode C, Ahmadian M and Taheri S 2010 Effective energy harvesting devices for railroad applications *Proc. SPIE* **7643** 76430X

[6] Scruggs J T and Jacob P 2009 Harvesting ocean wave energy *Science* **323** 1176–8

[7] Ni T, Zuo L and Kareem A 2011 Assessment of energy potential and vibration mitigation of regenerative tuned mass dampers on wind excited tall buildings *Proc. ASME IDETC* 48728

[8] Stanton S C, Erturk A, Mann B P and Inman D J 2010 Nonlinear piezoelectricity in electroelastic energy harvesters: modeling and experimental identification *J. Appl. Phys.* **108** 074903

[9] Cassidy I L, Scruggs J T, Behrens S and Gavin H P 2011 Design and experimental characterization of an electromagnetic transducer for large-scale vibratory energy harvesting applications *J. Intell. Mater. Syst. Struct.* **22** 2009–24

[10] Lefeuvre E, Audigier D, Richard C and Guyomar D 2007 Buck-boost converter for sensorless power optimization of piezoelectric energy harvester *IEEE Trans. Power Electron.* **22** 2018–25

[11] Ward J K and Behrens S 2008 Adaptive learning algorithms for vibration energy harvesting *Smart Mater. Struct.* **17** 035025

[12] Liu Y, Tian G, Wang Y, Lin J, Zhang Q and Hofmann H F 2009 Active piezoelectric energy harvesting: general principle and experimental demonstration *J. Intell. Mater. Syst. Struct.* **20** 575–85

[13] Scruggs J T, Cassidy I L and Behrens S 2011 Multi-objective optimal control of vibratory energy harvesting systems *J. Intell. Mater. Syst. Struct.* at press

[14] Stephen N G 2006 On energy harvesting from ambient vibration *J. Sound Vib.* **293** 409–25

[15] Scruggs J T 2010 On the causal power generation limit for a vibratory energy harvester in broadband stochastic response *J. Intell. Mater. Syst. Struct.* **21** 1249–62

[16] Ali S F, Adhikari S, Friswell M I and Narayanan S 2011 The analysis of piezomagnetoelastic energy harvesters under broadband random excitations *J. Appl. Phys.* **109** 074904

[17] Wonham W M and Cashman W F 1969 A computational approach to optimal control of stochastic saturating systems *Int. J. Control* **10** 77–98

[18] Gökçek C, Kabamba P T and Meerkov S M 2001 An lqr/lqg theory for systems with saturating actuators *IEEE Trans. Autom. Control* **46** 1529–42

[19] Narayanan S and Senthil S 1998 Stochastic optimal active control of a 2-dof quarter car model with non-linear passive suspension elements *J. Sound Vib.* **211** 495–506

[20] Ying Z G, Ni Y Q and Ko J M 2005 Semi-active optimal control of linearized systems with multi-degree of freedom and application *J. Sound Vib.* **279** 373–88

[21] Ni Y Q, Ying Z G, Yang J N and Spencer B F 2006 Stochastic optimal control of wind-excited tall buildings using semi-active mr-tlcds *Probab. Eng. Mech.* **19** 269–77

[22] Boyd S, Ghaoui L E, Feron E and Balakrishnan V 1994 *Linear Matrix Inequalities in System and Control Theory* (Philadelphia: SIAM)

[23] Kollmorgen 2010 Kollmorgen linear positioners catalog www.kollmorgen.com

[24] Kollmorgen 2010 Akm series motors www.kollmorgen.com

[25] Luenberger D G 1971 An introduction to observers *IEEE Trans. Autom. Control* **16** 596–602

[26] Roberts J B and Spanos P D 2003 *Random Vibration and Statistical Linearization* (New York: Dover)

[27] Wonham W M 1968 On a matrix riccati equation of stochastic control *SIAM J. Control* **6** 681–97

[28] Lewis F L and Syrmos V L 1995 *Optimal Control* (New York: Wiley-Interscience)

[29] Cassidy I L, Scruggs J T and Behrens S 2011 Optimization of partial-state feedback for vibratory energy harvesters subjected to broadband stochastic disturbances *Smart Mater. Struct.* **20** 085019

[30] Erickson R W 1997 *Fundamentals of Power Electronics* (London: Chapman and Hall)

[31] Advanced Motion Controls 2010 Analog drives for servo systems www.a-m-c.com